www.MaterialsViews.com

ADVANCED
FUNCTIONAL
MATERIALS
www.afm-journal.de

FULL PAPER

X-Ray Spectroscopic Investigation of Chlorinated Graphene: Surface Structure and Electronic Effects

Xu Zhang, Theanne Schiros,* Dennis Nordlund, Yong Cheol Shin, Jing Kong, Mildred Dresselhaus,* and Tomás Palacios*

Chemical doping of graphene represents a powerful means of tailoring its electronic properties. Synchrotron-based X-ray spectroscopy offers an effective route to investigate the surface electronic and chemical states of functionalizing dopants. In this work, a suite of X-ray techniques is used, including near edge X-ray absorption fine structure spectroscopy, X-ray photoemission spectroscopy, and photoemission threshold measurements, to systematically study plasma-based chlorinated graphene on different substrates, with special focus on its dopant concentration, surface binding energy, bonding configuration, and work function shift. Detailed spectroscopic evidence of C–Cl bond formation at the surface of single layer graphene and correlation of the magnitude of p-type doping with the surface coverage of adsorbed chlorine is demonstrated for the first time. It is shown that the chlorination process is a highly nonintrusive doping technology, which can effectively produce strongly p-doped graphene with the 2D nature and long-range periodicity of the electronic structure of graphene intact. The measurements also reveal that the interaction between graphene and chlorine atoms shows strong substrate effects in terms of both surface coverage and work function shift.

1. Introduction

Graphene, a 2D gapless semiconductor, has emerged as a promising material in a broad spectrum of applications in the era of post-silicon electronics.[1] One important reason that accounts for the great impact of silicon is the fact that the doping level in silicon can be engineered in a highly controllable way through ion implantation. In order to unleash the full potential of graphene electronics, it is also essential to find the best doping approach and to understand the doping mechanism and its effect on the unique electronic structure of graphene. Due to its 2D nature, graphene is truly an all-surface material. Consequently, surface functionalization can have a direct impact on its intrinsic characteristics, and therefore provides a powerful tool to engineer its electronic and structural properties. Plasma-based chlorination has been demonstrated to be an effective hole doping method, with the capability of maintaining a high mobility up to 1500 cm^2 V^{-1} s^{-1} in chemical vapor deposition (CVD)-grown graphene.[2–6] This is a great advantage over other doping approaches, such as fluorination and hydrogenation.[7–10] Furthermore, first principles density functional theory (DFT) calculations predict that a band gap of up to 1.21 eV can be opened in double-sided fully chlorinated graphene (CCl).[11,12] Chlorination has also been demonstrated in other carbon-based materials, such as carbon nanotubes,[13] graphite,[14,15] graphite oxide (GO),[16] Janus graphene,[17] and nanographenes,[18] manifesting various electronic applications such as lithium-ion batteries, transparent conducting films, and electrochemical devices. Several different chlorination methods have been successfully developed, including photochlorination,[4,13,19] cyclic chlorine trapping,[20] direct exfoliation,[21] electrophilic substitution,[18] and plasma-based chlorination.[2,3] High coverage (C$_{2.2}$Cl) of adsorbed chlorine on single-sided graphene was recently realized experimentally,[2] which paved the road to realize double-sided chlorinated graphene and could ultimately enable band gap engineering. However, the local electronic structure of chlorinated graphene, the nature of the C—Cl bonds, and the effect of chlorination on graphene's work function are still not well understood.

Synchrotron-based X-ray spectroscopy provides a sensitive probe of the chemical and electronic state of dopant species

X. Zhang, Prof. J. Kong, Prof. M. Dresselhaus,
Prof. T. Palacios
Department of Electrical Engineering and
Computer Science
Massachusetts Institute of Technology
Cambridge, MA 02139, USA
E-mail: millie@mgm.mit.edu; tpalacios@mit.edu
Dr. T. Schiros
Energy Frontier Research Center (EFRC)
Columbia University
New York, NY 10027, USA
E-mail: ts2526@columbia.edu
Dr. D. Nordlund
Stanford Synchrotron Radiation Lightsource
SLAC National Accelerator
Laboratory
Menlo Park, CA 94025, USA
Dr. Y. C. Shin
Department of Materials Science and Engineering
Massachusetts Institute of Technology
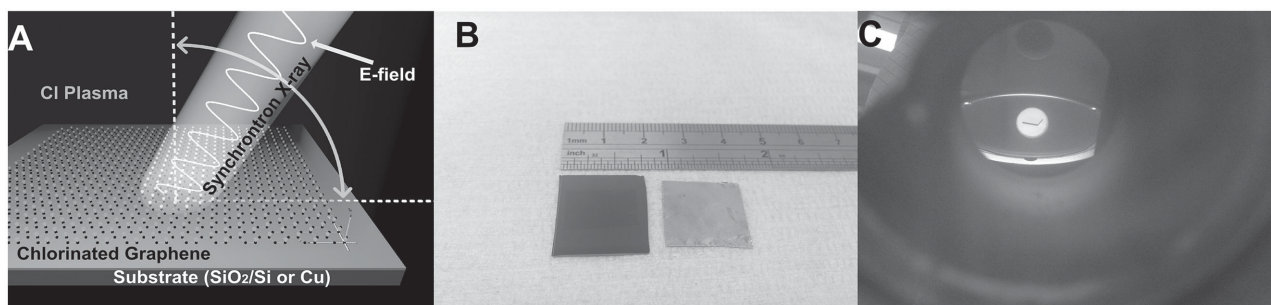Cambridge, MA 02139, USA

FULL PAPER

Figure 1. A) Illustration of synchrotron NEXAFS characterization of chlorinated graphene on different substrates, with tunable incident angles of E field. B) Images of CVD-grown graphene on different substrates (left: Si wafer capped with 300 nm SiO_2, right: 25 μm thick copper foil). C) Image of CVD-grown graphene treated in the chlorine plasma chamber.

even at the subpercent level,[4,5,22–26] thanks to its high flux and energy resolution, tunable wavelength, and polarization. Recent work based on carbon and nitrogen core-level X-ray spectroscopy, including near edge X-ray absorption fine structure (NEXAFS) and X-ray photoemission spectroscopy (XPS), successfully revealed an atom-specific picture of nitrogen-doped single layer graphene and provided detailed information on its dopant concentration, bond type and orientation, and corresponding work function shifts.[22]

In the present work, we carry out systematic chlorine plasma treatment on CVD-grown monolayer graphene samples and characterize the dopant surface coverage, bond configuration, and work function shifts using angle-resolved carbon K-edge (C 1s) NEXAFS, C 1s and Cl 2p XPS, and photoemission threshold measurements. The presence of adsorbed chlorine atoms introduces clear peaks into the XPS spectra, from which we quantify the coverage of C—Cl bonds on SiO_2/Si substrates to be 17%–38%, depending on the dc bias applied in the Cl plasma chamber. This concentration of adsorbed chlorine on the graphene surface is high enough to generate a distinct NEXAFS resonance at ≈286.2 eV for plasma-treated samples, corresponding to the 1s → π^* transition for C—Cl bonds. It is remarkable that a sharp core–hole exciton resonance at ≈291.85 eV is observed even after chlorination treatment, a spectroscopic fingerprint that long-range periodicity in the electronic structure of graphene is maintained after doping. The plasma-based chlorination is a highly nonintrusive doping approach: there is no significant buckling or other defects created in the graphene lattice and populated by the Cl atoms. It is a striking uniqueness of this doping approach, compared with other doping methods, such as nitrogen plasma,[27] hydrogenation,[9,10,28] and fluorination,[6,7] which introduce significant vacancies and local carbon sp³ hybridization. In the present work, a strong substrate effect is also found and studied: the Cl plasma interacts with graphene very differently in terms of both the surface coverage and the concentration-dependent work function shift, depending on whether the graphene sits on copper foil or on SiO_2/Si.

2. Results and Discussion

2.1. XPS Characterization Results

We systematically performed plasma-based chlorination treatment on CVD-grown graphene samples under different dc

bias conditions, on both SiO_2/Si and copper substrates (see the Experimental Section). XPS provides a surface-sensitive, element-specific spectroscopic tool to quantitatively measure the local coordination environment, yielding determinative information on atomic concentration. **Figure 1** shows our experimental setup and pictures of CVD-grown graphene samples. **Figure 2**A shows the C 1s XPS data for the untreated graphene samples and chlorinated graphene as a function of dc bias (4–20 V). The dc bias controls the acceleration toward the substrate and thus the kinetic energy of the chlorine when impinging on the graphene surface (see the Experimental Section and the Supporting Information). The main asymmetric peak observed at 284.5 eV binding energy is characteristic of C═C bonds in graphitic carbon.[29] After chlorine plasma treatment, a prominent photoemission peak appears at ≈286.6 eV due to the formation of C—Cl bonds, as observed in previous reports.[3,4,6] This peak does not appear in the untreated graphene samples, further confirming the formation of C—Cl bonds. The weak peak at ≈288.5 eV is due to a small amount of carbonyl groups, such as O—C═O, from contamination. Detailed peak fitting analysis can be found in Figure S4 (Supporting Information). The Cl 2p XPS spectra (spin–orbit split into $2p_{3/2}$ (200.6 eV) and $2p_{1/2}$ (202.2 eV) peaks) for the same chlorinated samples in Figure 2B show clear evidence of chlorine on the graphene samples; no Cl 2p intensity is observed for the untreated (pristine graphene) samples. Comparison of C 1s and Cl 2p photoemission intensity, normalized using tabulated photoionization cross sections of chlorine and carbon,[30,31] allows us to quantify the total chlorine coverage on the plasma-treated samples, as summarized in **Table 1**. The results confirm the existence of a significant amount of Cl atoms on the graphene, with the percent coverage of 17%–38%, depending on dc bias, roughly consistent with the data in our previous publication.[2] Here, we define the Cl coverage as the number of chlorine atoms divided by the number of carbon atoms. Figure 2C shows the total XPS area measured at four different spots on the sample surface for C 1s, Cl 2p, O 1s, and Si 2p core level spectra at different excitation energies used to estimate the Cl coverage (see the Experimental Section). The data show a consistent progression of Cl coverage (and associated "masking" of C 1s signal relative to pristine graphene), with highest coverage for the low dc bias (4–8 V) in agreement with previous report.[2] We also note that the amount of oxygen contamination on the surface is very low.
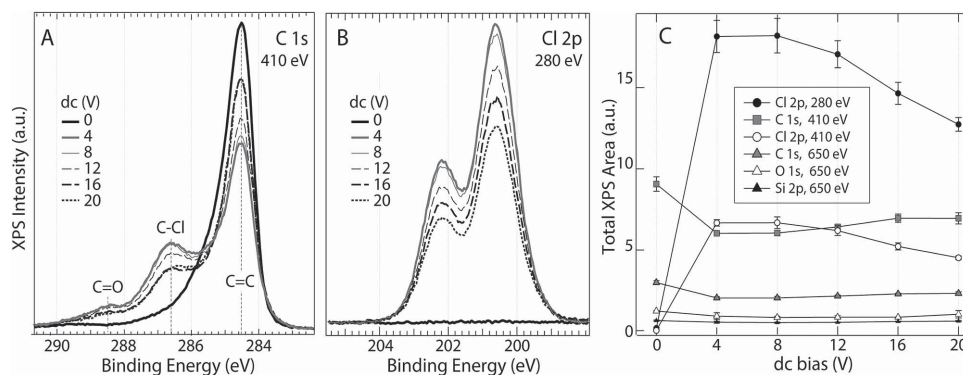
www.MaterialsViews.com

ADVANCED
FUNCTIONAL
MATERIALS
www.afm-journal.de

FULL PAPER

Figure 2. XPS measurements of pristine graphene and chlorinated graphene on SiO$_2$/Si treated at different dc bias. A) C 1s XPS data. The C—Cl bonds centered at 286.6 eV did not exist in the pristine graphene (black line), and only developed after Cl treatment. B) Cl 2p XPS data. The Cl 2p spin–orbit split (2p$_{3/2}$ (200.6 eV) and 2p$_{1/2}$ (202.2 eV)) peaks appear only after Cl treatment. C) Total XPS area (after Shirley background subtraction) for C 1s, Cl 2p, O 1s, and Si 2p core level spectra at different excitation energies; the average values of the XPS area of four different spots on each sample are shown with root mean square error bars (vertical lines through each data point).

2.2. NEXAFS Characterization Results

Angle-dependent NEXAFS measurements were performed on the as-prepared samples (see Figure 1A and the Experimental Section). **Figure 3** shows the carbon K-edge (C 1s) NEXAFS spectra measured in the total electron yield (TEY) mode for pristine graphene (dc = 0 V) and graphene samples that are transferred to SiO$_2$ substrates and then chlorinated under different dc bias (dc: 4–20 V). The strong peak at 285.4 eV (π*) is attributed to the resonance with the conduction π states around the M point in the Brillouin zone, and the σ* resonance at 293 eV is associated with the transition near the Γ point in the Brillouin zone.[32,33]

The adsorbed chlorine coverage on graphene is high enough to introduce a new resonance peak in the NEXAFS data around 286.2 eV, which we assign to the surface C—Cl bonds formed with chlorination treatment (Figure 3). The C—Cl resonance (286.2 eV) is observed for all Cl-treated graphene samples under different dc bias, and does not appear in untreated (pristine) graphene. The peak gives direct evidence of the formation of C—Cl bonds during the Cl plasma treatment and information on their bonding characters. We note that in XPS (in a fully ionized final state) the C 1s peak associated with C—Cl is shifted by about 2 eV to higher binding energy, reflecting the electron withdrawing effect of the adsorbed chlorine due to the higher electronegativity of Cl (3.16 on the Pauling scale) compared to C (2.55 on the Pauling scale).[34] The higher energy ($\approx$0.8 eV) NEXAFS resonance associated with C—Cl is consistent with the electron withdrawing effect of the Cl, but it also indicates a final

state relaxation that lowers the final state energy in NEXAFS relative to the fully ionized XPS case. This indicates that the C—Cl states we observe in NEXAFS are more local in character relative to the extended π* network, which will provide additional screening of the core–hole in the final state and lower its binding energy relative to the ionization potential as observed in XPS.

Aside from the electron withdrawing effect, the C 1s NEXAFS (Figure 3) shows that the adsorbed chlorine does not significantly disrupt the graphitic network or introduce defects when prepared under the described conditions. For both chlorinated and pristine graphene, a strong (and opposite) angular dependence is observed for both the π* and σ* peaks of the C=C bonds as we change the incident angle of the X-ray beam relative to the graphene surface, and therefore the orientation of the E-field vector of the incoming (polarized) X-ray beam relative to the highly oriented π and σ orbitals of the 2D carbon sheet (Figures 1A and 3). A sharp core–hole excitonic feature at 291.85 eV (Figure 3) is a characteristic indicator of long-range periodicity of the electronic structure of our pristine graphene; this feature is observed for highly ordered pyrolytic graphite (HOPG)[29,35] and high quality pristine graphene.[22,23] Thus, surprisingly, the chlorine treatment neither significantly buckles the graphene lattice nor disrupts the graphitic network. Our chlorination treatment results in highly nonintrusive doping; the spectroscopic data indicate that no significant defects are created and populated by the chlorine dopants.

Moreover, in contrast to the strong angular dependence of the C=C π* peak (285.4 eV), characteristic of planar graphitic

Table 1. Atomic Cl coverage (% Cl) on SiO$_2$/Si substrates compared with on copper foil substrates under different dc bias treatment. The upper and lower limits of the chlorine coverage range shown for graphene on SiO$_2$/Si substrates are estimated by comparing XPS intensity (normalized by the atomic sensitivity factor at the photon energy used[30,31] measured at photon energies of 280 eV for Cl 2p and 410 eV for C 1s (upper limit) and 650 eV for both Cl 2p and C 1s (lower limit), respectively (details provided in the Experimental Section). We note that for graphene on SiO$_2$/Si substrates, the values in the table reflect the coverage of adsorbed chlorine on the graphene surface, while on copper foil, the total Cl concentration is distributed between adsorbed chlorine and chlorine atoms which have diffused into the foil substrate and bonded to Cu (see Figure 4B and corresponding discussion).

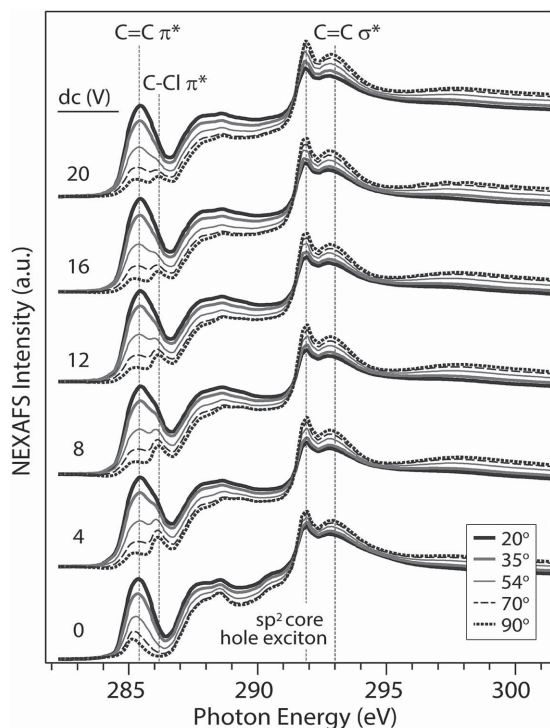| Substrate	dc = 0 V	dc = 4 V	dc = 8 V	dc = 12 V	dc = 16 V	dc = 20 V
SiO$_2$/Si	0	29.0%–38.0%	29.0%–38.0%	25.4%–33.2%	20.2%–25.9%	17.3%–22.5%
Copper foil	0	7.1%	7.2%	5.4%	6.8%	5.6%

Figure 3. Angle-dependent C 1s NEXAFS measurements for graphene transferred to SiO_2/Si as a function of dc bias during chlorine treatment. Note: dc = 0 V corresponds to pristine (untreated) graphene. The peak around 285.4 eV corresponds to the resonance with the conduction π states at the M point in the Brillouin zone. The σ^* resonance at 293 eV is associated with the transition near the Γ point in the Brillouin zone.[32,33] The new resonance peak at 286.2 eV is attributed to the C—Cl bonds formed due to the chlorination, which appears in all Cl-treated graphene samples under different dc bias, and does not appear in untreated (pristine) graphene.

carbon bonds, peak fitting analysis reveals the intensity of the C—Cl NEXAFS bond resonance (286.2 eV) is relatively invariant with changes in incident angle (see Figure S3, Supporting Information). This indicates that the average azimuthal orientation of the C—Cl bonds is fairly isotropic, or that the chemical C—Cl bond is associated with states of local character which have their p-like orbitals (e.g., π orbitals) at an angle close to 55° relative to the surface normal where azimuthally averaged angular dependence will also disappear.[29] (We note that any apparent change in intensity of the C—Cl π^* with incident angle is a by-product of the strong variation in C=C π^* intensity due to the closeness in energy of the two resonances at 285.4 and 286.2 eV (see Figure S3, Supporting Information).

Compared with the NEXAFS spectra for chlorinated graphene on copper substrates (see Figure S2, Supporting Information), the Cl/G/SiO$_2$ samples exhibit much cleaner spectra in the range between 287.4 and 288.5 eV, with an intensity mainly due to C=C and C—Cl resonances as opposed to C—O and C—H species which also appear in this range. This suggests that a higher Cl coverage helps to protect the surface from contamination of C—H bonds (≈287 eV), carbonyl C=O bonds (≈≥288 eV), and others, and therefore results in a cleaner graphene surface.

It is remarkable that this high coverage of adsorbed chlorine (17%–38%) does not introduce significant buckling or distortion of the graphene lattice. This is evidenced by the strong angular dependence of the C 1s σ^* and π^* NEXAFS spectra and the presence of the sharp core–hole exciton feature at 291.85 eV, both of which are essentially unperturbed by the chlorine treatment. Aside from the appearance of the C—Cl π^* peak at 286.2 eV, the C 1s NEXAFS spectra are almost identical before and after chlorination and are spectroscopic signatures of sp^2-hybridized carbon. This similarity strongly indicates that our plasma-based chlorination is a unique surface functionalization, while introducing states that are unique to the C—Cl bonds, does not produce any significant defect or buckling. Thus, the overall crystallinity and extended band structure of graphene remains uninterrupted. This is consistent with the transport studies of chlorinated graphene, which demonstrated that, after chlorination, the carrier mobility in CVD graphene can still be maintained at ≈1500 cm^2 V^{-1} s^{-1}[2] and its sheet resistance can be reduced due to a significant hole doping effect.[2,3] We also note that the chlorinated graphene presented here is particularly well suited for angle-resolved photoemission spectroscopy (ARPES) studies for which a well-ordered system is needed to obtain high resolution in momentum space, for which the π dispersion and potential band opening could be observed.

2.3. Substrate Effects

For comparison, we also studied CVD-grown graphene on copper (without transfer) under identical plasma conditions and repeated the synchrotron measurements. **Figure 4**A,B shows the corresponding C 1s and Cl 2p XPS spectra, respectively, under different dc bias. The features in the C 1s spectra (Figure 4A) are in good agreement with that for chlorinated graphene on SiO$_2$ substrates, however the peak intensity ratio is quite different. As for the chlorinated graphene sheets on SiO$_2$/Si substrates (Figure 2), the chlorinated graphene on Cu foil samples show an asymmetric C 1s photoemission peak at 284.5 eV, the spectral fingerprint of graphitic C=C bonds, and a weak peak at ≈288.5 eV due to O—C=O bonds from the carbon oxide residues. Detailed peak fitting analysis can be found in Figure S5 (Supporting Information). Likewise, the degree of oxygen contamination is low for both chlorinated graphene on Cu foil (Figure 4A) and for graphene transferred to SiO$_2$/Si (Figure 2A). A small shoulder on the high binding energy side of the main C=C peak, broadly centered at ≈286.5 eV appears after chlorine plasma treatment, due to the formation of C—Cl bonds (Figure 4A and inset). However, the C—Cl peak intensity is much weaker than the one observed for samples on SiO$_2$/Si substrates after chlorination treatment (Figure 2B), indicating a much lower coverage of adsorbed chlorine for graphene on the copper foil substrates.

In fact, the Cl 2p XPS spectra for chlorinated graphene on the copper foil shown in Figure 4B looks quite different from the corresponding spectra for graphene on SiO$_2$/Si. The XPS intensity from adsorbed chlorine is again observed at ≈200.6 and 202.2 eV (Cl 2p$_{3/2}$ and Cl 2p$_{1/2}$, respectively), as for the transferred samples (Figure 2B). However, in striking contrast to the Cl/G/SiO$_2$ samples, the Cl 2p XPS for Cl/G/Cu samples shows an additional strong peak at ≈198.8 eV binding energy

www.MaterialsViews.com

ADVANCED
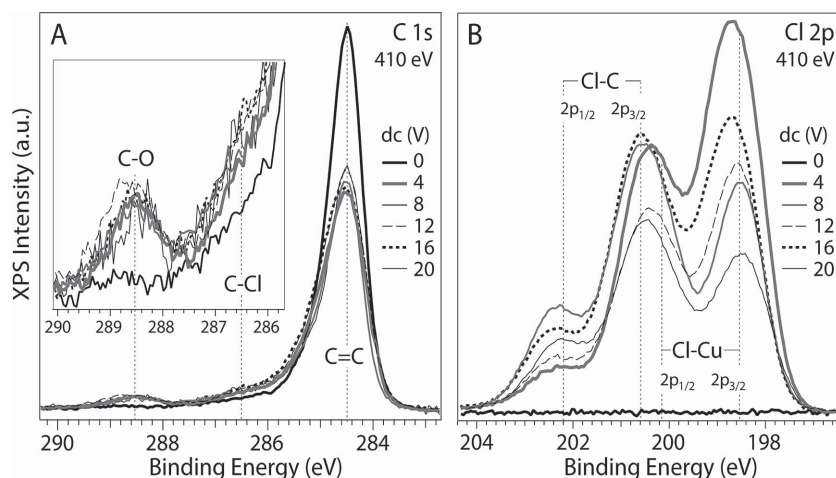FUNCTIONAL
MATERIALS
www.afm-journal.de

FULL PAPER

Figure 4. A) C 1s and B) Cl 2p XPS data, representing the average of 11 positions on the surface of chlorinated graphene on copper substrates with excitation energy $h\nu = 410$ eV, for samples prepared with different bias conditions (0–20 V). The Cl 2p spectra show that a significant portion of the total chlorine signal comes from chlorine bonded to the Cu foil substrates. Despite the presence of both Cl—C and Cl—Cu bonds, the atomic coverage of chlorine in these samples is significantly lower than observed for graphene transferred to SiO$_2$/Si after plasma treatment, as shown in Table 1.

and a broadening of the peak at ≈200.6 eV, with greater variation in the binding energy of the peak center; no chlorine signal is observed for pristine graphene on copper foil (Figure 4B). We interpret these differences as arising from the Cl 2p$_{3/2}$ and Cl 2p$_{1/2}$ components at ≈198.8 and ≈200.2 eV, respectively, of Cl—Cu bonds. The proximity of the latter to the Cl 2p$_{3/2}$ peak of adsorbed chlorine on graphene effectively broadens and shifts this peak to lower binding energy. The assignment of the additional features for Cl/G/Cu to Cl—Cu bonds is supported by the facile diffusion of chlorine in copper foils above 10^{-2} Torr, and in precise agreement with the binding energy of ClCu compounds measured in a previous report.[36]

By calculating the ratio of the C—Cl peak area in Cl 2p to the C peak area in C 1s after taking the atomic sensitivity factors into consideration,[30] we estimated the total atomic chlorine coverage for Cl plasma treated graphene on copper substrates (Table 1). It is worth noting that the Cl coverage reported here for the Cl/G/Cu samples is the total chlorine contribution, which contains signals from both the C—Cl bonds and Cu—Cl bonds formed during the plasma treatment. The total concentration of chlorine in the Cl/G/Cu samples is significantly smaller than the corresponding values for the ones on SiO$_2$/Si substrates, and only a portion of this signal is due to the formation of C—Cl bonds. This is consistent with the much weaker C—Cl XPS peak for Cl/G/Cu in the C 1s XPS (Figure 4A) compared to Cl/G/SiO$_2$ (see Figure 2A). We also studied the NEXAFS spectrum of the Cl/G/Cu samples (Figure S2, Supporting Information), qualitatively showing similar results as Cl/G/SiO$_2$. However, no clear C—Cl resonance peak can be observed (see the Sup-

porting Information), probably due to the relatively low coverage of C—Cl and the much weaker interaction between Cl and G/Cu. All of these observations indicate that the interaction between the Cl plasma and graphene highly depends on the substrate environment.

The photoemission threshold measurements enabled us to quantify the shift of the work function in graphene as a result of the chlorine doping effect. As shown in **Figure 5**, the chlorination treatment shifted the photoemission threshold to the positive side (see the Supporting Information for details), and the amount of the shift depends on the dc bias applied. This indicates a p-doping effect, which is consistent with previous transport results in the literature.[2,3] For both copper and SiO$_2$/Si substrates, the change in the photoemission threshold saturates after the dc bias is beyond 8 V. However, the substrate effect on the work function shift due to Cl doping is significant: for graphene on copper, its Fermi level E_F is shifted downward by about 0.35 eV, while for graphene on SiO$_2$/Si substrates, the much (≈4–5 times) higher chlorine concentration causes E_F to shift downward by about 0.9 eV. This work clearly shows that the plasma-based chlorination is a highly effective p-doping approach for graphene. Not surprisingly, the magnitude of p-doping closely follows the chlorine coverage, which, quite unexpectedly, is much higher for graphene on SiO$_2$/Si substrates than on copper substrates.

2.4. Discussion

In summary, the experimental data reveal a high coverage of chemically bonded Cl is present with significant electron withdrawing effect (XPS and photoemission threshold
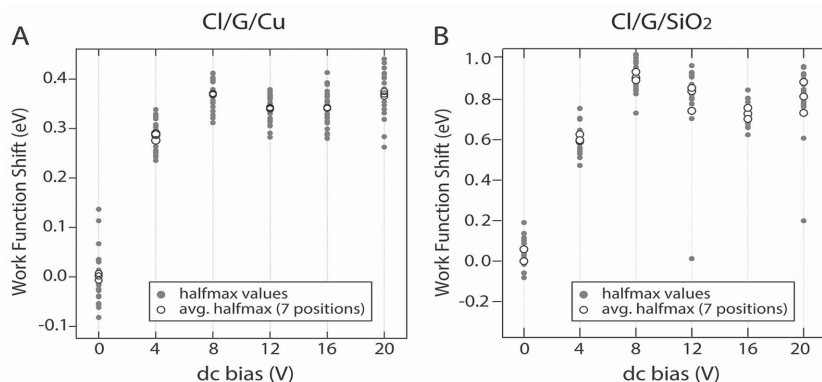

Figure 5. Photoemission threshold measurements for chlorinated graphene on A) copper and B) SiO$_2$/Si. The photoemission cut-off shifts to lower binding energy with chlorination, consistent with the higher work function (due to p-doping). The work function shift (y-axis) is obtained from measurement of the electron kinetic energy at the photoemission threshold relative to pristine graphene (PG or dc = 0); the plots show the halfmax value for 21 total measurements on each sample (solid red circles) obtained from three measurements at seven positions on the graphene surface and the average halfmax (open black circles) of seven positions.

FULL PAPER

measurement) that is forming hybridized states which have local character (NEXAFS). Yet the bonding is not disruptive to the overall electronic structure of the graphene that remains highly ordered and without significant defects and buckling (NEXAFS). Even though we cannot formulate a precise chemical bond configuration that explains our observations, we have learned from the combined experimental evidences, that the chemical C—Cl bond has the following characters:

1) The Cl is primarily bonded to the graphene lattice carbon and not just on grain boundaries and defects based on the minimal introduction of defects during chlorination, the pertained angular dependence in the π^* and σ^* bands, the presence of the core-exciton that is sensitive to long-range order, and the high fraction of C—Cl bonds observed.
2) The Cl—C bond involves significant charge transfer effect from the graphene lattice to chlorine, leading to strong p-doping of the lattice as observed by the chemical shift in XPS and the large work function change (photoemission threshold measurement).
3) The chemical bond is either formed on a single site, or for bonding geometries that provide a narrow distribution of chemical shift in the ionized state (Cl 2p XPS and C—Cl states in C 1s NEXAFS).
4) The chemical bond is associated with states of local character that either have their p-like orbital states at an angle close to the magic angle (near 55°) relative to the surface normal, or a distribution of that gives an isotropic angular dependence in the C 1s NEXAFS data.
5) All of the above must be true without introducing significant changes neither to the local sp² network nor the long-range order, as indicated by C 1s NEXAFS.

These intriguing results are important experimental observations, but it cannot easily be translated into a detailed chemical bonding picture without further investigation. For example, we would expect that a well-defined absorption geometry (e.g., single sided on top) would display a well-defined angular dependence and also, if covalently bonded, enforcing departure from a well-defined local sp² environment. We anticipate that theoretical simulations of NEXAFS transitions and XPS binding energies for a number of different local Cl absorption sites (which is outside the scope of this report), directed by previous theoretical work[11,12] on Cl–graphene absorption and analyzed with respect to anisotropy and energetics, are needed to reveal a more detailed microscopic picture of the C—Cl bonds and disentangle the associated orbital hybridization around the carbon sites. To this end, additional experimental evidence of covalency, bond length, and band structure from future ARPES and extended X-ray absorption fine structure spectroscopy (EXAFS) would be of great value.

3. Conclusion

We systematically studied the plasma-based chlorination treatment on CVD-grown graphene on different substrates through NEXAFS and XPS characterizations. The NEXAFS and XPS spectra confirmed the formation of the C—Cl bonds and their bonding characters. We observed a high density of C—Cl bonds

without significant increase of defects or major interruption of the overall graphene electronic structure. It is found that the distinct sp² carbon core–hole exciton retained its sharpness even after the chlorination treatments, which indicates that the plasma-based chlorination can largely preserve the long-range periodicity in the graphene lattice. This distinguished our chlorination approach as a noninvasive and effective doping method, compared to other alternative approaches. The interaction between chlorine plasma and graphene exhibits strong substrate effects, in terms of both Fermi level shift and surface coverage. The use of SiO_2/Si substrates enables more than ≈4–5 times higher Cl atoms coverage on the graphene surface than on copper foils. Photoemission threshold measurements show that the Cl plasma p-doping can shift the Fermi level in graphene downward by about 0.9 eV when SiO_2/Si is used as supporting substrates. As a comparison, for chlorinated graphene on copper (Cl/G/Cu), its Fermi level is shifted downward by about 0.35 eV.

4. Experimental Section

Growth and Transfer of Graphene: Graphene samples were synthesized by established low pressure CVD (LPCVD) process on Cu foils, in a mixture gas of H_2 and CH_4. The growth temperature and pressure were maintained at 1035 °C and at 1.70 Torr, respectively. The Cu foil was treated with a nickel etchant (Nickel Etchant TFB, Transense) at first before the synthesis process in order to obtain a better morphology of graphene. Then, uniform monolayer graphene was successfully synthesized on the Cu substrate. While a half piece of the synthesized graphene/Cu sample was quickly transferred from the growth chamber to a vacuum chamber to avoid the adsorption of impurities or oxidation, the graphene of the other half piece was transferred onto a Si wafer capped with 300 nm SiO_2, using the PMMA-supported wet-transfer process.

Plasma-Based Chlorination Treatment: An electron cyclotron resonance reactive ion etcher (ECR/RIE, PlasmaQuest) was used to chlorinate graphene samples. The ECR power and dc bias in the chamber to finely control the chlorination parameters were carefully optimized. Before each run, oxygen plasma was activated to clean the chamber for 10 min. And then, the desired chlorine plasma recipe was run for another 10 min to properly condition the chamber, before treating the real samples with plasma. Both the pressure and flow rate of chlorine gas were kept at constant values (pressure: 20 m Torr, flow rate: 80 sccm). The ECR power used was 100 W. The dc bias was varied from 4 to 20 V. All the experiments were done at 30 °C for 1 min. The facility has two alternative controlling knobs to tune the Cl plasma energy: rf power and dc bias. It was found that controlling dc bias allows to more finely tune the plasma energy and can generate Cl plasma at a much lower power level than by controlling the rf power. Moreover, at lower dc bias, the kinetic energy of the impinging Cl ions was reduced and therefore the bombardment on the graphene surface resulting in less defects can be minimized. The lowest limit that can be run in the ECR plasma facility is dc = 4 V. Also, special attention is paid to minimize the air exposure during the sample preparation and plasma treatment process. A clean surface of chlorinated graphene is important for NEXAFS measurement. After chlorination, the sample can be kept under ambient condition at room temperature for about two to three weeks before significant Cl desorption is observed.

Core Level Spectroscopy: NEXAFS and XPS measurements were performed at the wiggler source beamline 10-1 at the Stanford Synchrotron Radiation Lightsource (SSRL), in an ultrahigh vacuum (better than 10^{-9} Torr) endstation designed for surface and solid state experiments. The reference absorption intensity (I_0) of the incoming X-ray beam, measured on a gold-coated mesh positioned just after the

www.MaterialsViews.com

ADVANCED
FUNCTIONAL
MATERIALS
www.afm-journal.de

FULL PAPER

refocusing optics, was measured simultaneously and used to normalize the spectra to avoid any artifact due to beam instability. Polarization-dependent C 1s NEXAFS data were obtained by changing the angle between the incoming X-ray beam and the sample stage from near-parallel 20° and normal (90°) incidence; up to seven measurements were taken at each incident angle for four different positions on the sample surface. A linear background was subtracted as determined from a region before the absorption edge and the spectra were normalized in the postcontinuum region between 320 and 330 eV. Carbon K-edge NEXAFS collection was performed in the partial electron yield (PEY) mode, with a grid bias of −200 V, selected to optimize both the surface sensitivity of the measurement and the TEY mode, which measures the total drain current from the sample. XPS measurements were obtained at multiple photon energies to improve the statistics on the quantification of the adsorbed chlorine concentration and to obtain a nondestructive depth profile of the atomic concentration ratios. SSRL beamline 10-1 has a spherical grating monochromator and the focused beam has a spot size of less than 1 mm^2. Measurements were repeated at multiple spots across the sample surface (at least four for XPS and NEXAFS measurements, and 20 for photoemission threshold measurements).

Supporting Information

Supporting Information is available online from the Wiley Online Library or from the author.

Acknowledgements

[1] K. S. Novoselov, A. K. Geim, S. V. Morozov, D. Jiang, Y. Zhang, S. V. Dubonos, I. V. Grigorieva, A. A. Firsov, *Science* **2004**, *306*, 666.

[2] X. Zhang, A. Hsu, H. Wang, Y. Song, J. Kong, M. S. Dresselhaus, T. Palacios, *ACS Nano* **2013**, *7*, 7262.

[3] J. Wu, L. Xie, Y. Li, H. Wang, Y. Ouyang, J. Guo, H. Dai, *J. Am. Chem. Soc.* **2011**, *133*, 19668.

[4] B. Li, L. Zhou, D. Wu, H. Peng, K. Yan, Y. Zhou, Z. Liu, *ACS Nano* **2011**, *5*, 5957.

[5] N. A. Vinogradov, K. A. Simonov, A. V. Generalov, A. S. Vinogradov, D. V. Vyalikh, C. Laubschat, N. Mårtensson, A. B. Preobrajenski, *J. Phys. Condens. Matter* **2012**, *24*, 314202.

[6] K. Gopalakrishnan, K. S. Subrahmanyam, P. Kumar, A. Govindaraj, C. N. R. Rao, *RSC Adv.* **2012**, *2*, 1605.

[7] S.-H. Cheng, K. Zou, F. Okino, H. R. Gutierrez, A. Gupta, N. Shen, P. C. Eklund, J. O. Sofo, J. Zhu, *Phys. Rev. B* **2010**, *81*, 205435.

[8] K.-J. Jeon, Z. Lee, E. Pollak, L. Moreschini, A. Bostwick, C.-M. Park, R. Mendelsberg, V. Radmilovic, R. Kostecki, T. J. Richardson, E. Rotenberg, *ACS Nano* **2011**, *5*, 1042.

[9] D. C. Elias, R. R. Nair, T. M. G. Mohiuddin, S. V. Morozov, P. Blake, M. P. Halsall, A. C. Ferrari, D. W. Boukhvalov, M. I. Katsnelson, A. K. Geim, K. S. Novoselov, *Science* **2009**, *323*, 610.

[10] J. O. Sofo, A. S. Chaudhari, G. D. Barber, *Phys. Rev. B* **2007**, *75*, 153401.

[11] M. Yang, L. Zhou, J. Wang, Z. Liu, Z. Liu, *J. Phys. Chem. C* **2011**, *116*, 844.

[12] H. ahin, S. Ciraci, *J. Phys. Chem. C* **2012**, *116*, 24075.

[13] L. Oliveira, F. Lu, L. Andrews, G. A. Takacs, M. Mehan, T. Debies, *J. Mater. Res.* **2014**, *29*, 239.

[14] V. A. Tur, A. V. Okotrub, Y. V. Shubin, B. V. Senkovskiy, L. G. Bulusheva, *Phys. Status Solidi B* **2014**, *251*, 2613.

[15] L. Wang, C. Guo, Y. Zhu, J. Zhou, L. Fan, Y. Qian, *Nanoscale* **2014**, *6*, 14174.

[16] J.-Y. Kim, W. H. Lee, J. W. Suk, J. R. Potts, H. Chou, I. N. Kholmanov, R. D. Piner, J. Lee, D. Akinwande, R. S. Ruoff, *Adv. Mater.* **2013**, *25*, 2308.

[17] L. Zhang, J. Yu, M. Yang, Q. Xie, H. Peng, Z. Liu, *Nat. Commun.* **2013**, *4*, 1443.

[18] Y.-Z. Tan, B. Yang, K. Parvez, A. Narita, S. Osella, D. Beljonne, X. Feng, K. Müllen, *Nat. Commun.* **2013**, *4*.

[19] L. Zhou, L. Zhou, M. Yang, D. Wu, L. Liao, K. Yan, Q. Xie, Z. Liu, H. Peng, Z. Liu, *Small* **2013**, *9*, 1388.

[20] V. P. Pham, K. N. Kim, M. H. Jeon, K. S. Kim, G. Y. Yeom, *Nanoscale* **2014**, *6*, 15301.

[21] H. L. Poh, P. Šimek, Z. Sofer, M. Pumera, *Chem. Weinh. Bergstr. Ger.* **2013**, *19*, 2655.

[22] T. Schiros, D. Nordlund, L. Pálová, D. Prezzi, L. Zhao, K. S. Kim, U. Wurstbauer, C. Gutiérrez, D. Delongchamp, C. Jaye, D. Fischer, H. Ogasawara, L. G. M. Pettersson, D. R. Reichman, P. Kim, M. S. Hybertsen, A. N. Pasupathy, *Nano Lett.* **2012**, *12*, 4025.

[23] L. Zhao, R. He, K. T. Rim, T. Schiros, K. S. Kim, H. Zhou, C. Gutiérrez, S. P. Chockalingam, C. J. Arguello, L. Pálová, D. Nordlund, M. S. Hybertsen, D. R. Reichman, T. F. Heinz, P. Kim, A. Pinczuk, G. W. Flynn, A. N. Pasupathy, *Science* **2011**, *333*, 999.

[24] L. Zhao, M. Levendorf, S. Goncher, T. Schiros, L. Pálová, A. Zabet-Khosousi, K. T. Rim, C. Gutiérrez, D. Nordlund, C. Jaye, M. Hybertsen, D. Reichman, G. W. Flynn, J. Park, A. N. Pasupathy, *Nano Lett.* **2013**, *13*, 4659.

[25] L.-S. Zhang, X.-Q. Liang, W.-G. Song, Z.-Y. Wu, *Phys. Chem. Chem. Phys.* **2010**, *12*, 12055.

[26] D. Geng, S. Yang, Y. Zhang, J. Yang, J. Liu, R. Li, T.-K. Sham, X. Sun, S. Ye, S. Knights, *Appl. Surf. Sci.* **2011**, *257*, 9193.

[27] R. Kurt, J.-M. Bonard, A. Karimi, *Carbon* **2001**, *39*, 1723.

[28] S. Rajasekaran, S. Kaya, F. Abild-Pedersen, T. Anniyev, F. Yang, D. Stacchiola, H. Ogasawara, A. Nilsson, *Phys. Rev. B* **2012**, *86*, 075417.

[29] J. Stöhr, *NEXAFS Spectroscopy, Springer Series in Surface Sciences*, Vol. 25, Springer, Berlin **1992**.

[30] J. J. Yeh, I. Lindau, *At. Data Nucl. Data Tables* **1985**, *32*, 1.

[31] D. E. Parry, *Rapid Commun. Mass Spectrom.* **1994**, *8*, 579.

[32] M. Papagno, A. F. Rodríguez, Ç. Ö. Girit, J. C. Meyer, A. Zettl, D. Pacilé, *Chem. Phys. Lett.* **2009**, *475*, 269.

[33] D. Pacilé, M. Papagno, A. F. Rodríguez, M. Grioni, L. Papagno, Ç. Ö. Girit, J. C. Meyer, G. E. Begtrup, A. Zettl, *Phys. Rev. Lett.* **2008**, *101*, 066806.

[34] D. R. Lide, *CRC Handbook of Chemistry and Physics: A Ready-Reference Book of Chemical and Physical Data*, CRC Press, **2004**.

[35] P. A. Brühwiler, A. J. Maxwell, C. Puglia, A. Nilsson, S. Andersson, N. Mårtensson, *Phys. Rev. Lett.* **1995**, *74*, 614.

[36] W. Sesselmann, T. J. Chuang, *Surf. Sci.* **1986**, *176*, 32.